Supporting Information for

Visible radiation-driven photomineralization and photoproduction of dissolved organic matter in a large estuary: Implications for coastal ocean biogeochemical cycles

Guisheng Song[1*], Fuxin Niu[2], Yao Gong[2], Philippe Massicotte[3], Han Zuo[1], Mengting Li[1], Huixiang Xie[4*]

[1]Tianjin Key Laboratory for Marine Environmental Research and Service, School of Marine Science and Technology, Tianjin University, Tianjin, China;

[2]Tianjin Ocean Center, Ministry of Natural Resources, Tianjin, China;

[3]CNRS – Université Laval – Sorbonne Université – Laboratoire de recherche international Takuvik, Québec, Canada;

[4]Institut des sciences de la mer, Université du Québec à Rimouski, Rimouski, Québec, Canada.

*Corresponding authors: G. Song (guisheng.song@tju.edu.cn) and H. Xie (huixiang_xie@uqar.ca)

Contents of this file

Text S1. Fraction of photons absorbed by CDOM in the water column

The fraction of photons absorbed by CDOM, $Q_{a,CDOM}(\lambda)$ (mol photons m^{-2} d^{-1}), in the euphotic zone at each station is calculated according to Equation S1:

$$Q_{a,CDOM}(\lambda) = Q(0,\lambda) \times R \times F(\lambda) \quad \text{(S1)}$$

where $Q(0,\lambda)$ (mol photons m^{-2} d^{-1}) is the monthly-averaged daily solar photon flux at the sea surface under clear-sky condition in the wavelength range of 290–600 nm over the PRE (22.5 °N) derived from the SMARTS2 model in January 2016;[1,2] R is the combination of two correction factors for light reflection by cloud (0.8) and at the air-water interface (0.93),[3] and F(λ) is the fraction of photons absorbed by CDOM at wavelength λ (nm). The wavelength-integrated $Q_{a,CDOM}(\lambda)$ in UVB (290–320 nm), UVA (320–400 nm) and VIS (400–600 nm) (Q_{UVB}, Q_{UVA}, and Q_{VIS}) are then calculated for estimating the relative contributions of UVB, UVA and VIS to PT in main text Equation 2.

F(λ), in the euphotic zone was calculated using the following equation:

$$F(\lambda) = \frac{a_{CDOM}(\lambda)}{a_{CDOM}(\lambda)+a_P(\lambda)+a_w(\lambda)} \quad \text{(S2)}$$

where $a_p(\lambda)$ (m^{-1}) and $a_w(\lambda)$ (m^{-1}) denote the absorption coefficients of particles and pure water,[4,5] respectively. $a_p(\lambda)$ was estimated from the suspended particulate matter (SPM) concentrations determined at the CDOM sampling stations in January 2016 (Sta. M01: 22.6 mg L^{-1}; M08: 50.9 mg L^{-1}; Sta. M10: 5.60 mg L^{-1})[6] and the linear relationships between $a_p(\lambda)$ and SPM (Figure S4A) established from the July 2013 data reported by Wang et al. (2014)[7], assuming negligible seasonal and interannual variabilities in the established $a_p(\lambda)$-SPM relationships. The calculated $a_p(\lambda)$ at Sta. M01, M08 and M10 decreases exponentially with increasing wavelength, following the function of $y = a \times e^{(-bx)} + c$ ($R^2 > 0.995$) (Figure S4B). Wang et al.'s $a_p(\lambda)$ data were limited to the wavelength range of 350–600 nm[7]. $a_p(\lambda)$ values from 290 to 349 nm were extrapolated from the regressed equation (Figure S4B).

Text S2. Modelling depth-resolved VIS-induced photoproduction of protein-like FDOM and CO_2 in the water column

As CO_2 is the dominant product of DOC photomineralization,[8-10] CO_2 photoproduction is quantitatively equivalent to DOC photomineralization. The depth-

resolved monthly photoproduction rates of protein-like FDOM and CO_2 in January 2016 (sampling season in this study) are estimated for the shelf Sta. M10 using Equation S3:

$$P = AQY(VIS) \times \int_{400}^{600} Q(z,\lambda) \times a_{CDOM}(\lambda) d\lambda \quad \text{(S3)}$$

P denotes the photoproduction rate of protein-like FDOM (P_{PFDOM}: R.U. L^{-1} d^{-1}) or CO_2 (P_{CO2}: μmol L^{-1} d^{-1}), AQY(VIS) the broadband AQY(VIS) of protein-like FDOM photoproduction (AQY_{PFDOM}(VIS)) or DOC photomineralization (AQY_{DOC}(VIS)), and $Q(z,\lambda)$ the spectral scalar photon flux at depth z (m) (mol photons m^{-2} d^{-1}), which is ~1.3 times the corresponding downwelling photon flux ($Q_d(z,\lambda)$) (Gordon 1989), which is computed as follows:

$$Q_d(z,\lambda) = Q_d(0,\lambda) \times \exp(-K_d(\lambda) \times z) \quad \text{(S4)}$$

$Q_d(0,\lambda)$ is $Q_d(z,\lambda)$ at the air-sea interface (z = 0 m), approximately equal to $Q(0,\lambda)$ in Equation S1, and $K_d(\lambda)$ is the diffusive attenuation coefficient (m^{-1}) estimated according to Morel (1974)[11] and Vodacek et al.(1994)[12]. Vertical homogeneity is assumed for AQY(VIS), $a_{CDOM}(\lambda)$ and $K_d(\lambda)$, and no wavelength-dependence for AQY(VIS). The vertical profiles of the monthly P_{PFDOM} and P_{CO2} are shown in Figure S5.

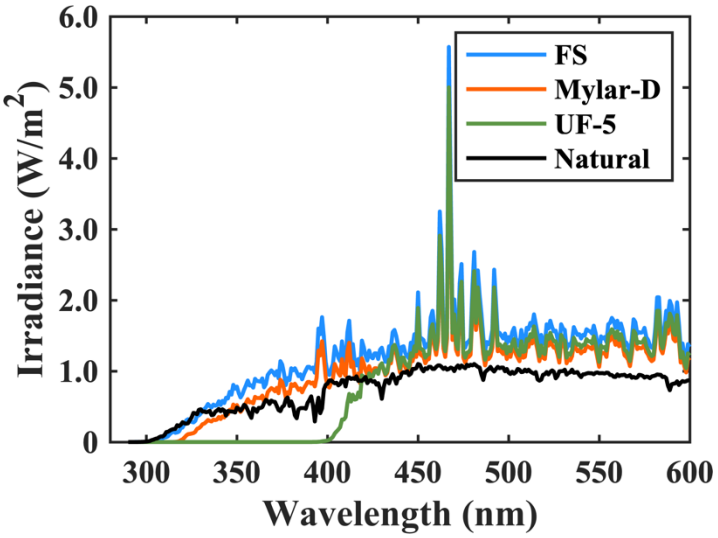

Figure S1. Measured spectral irradiances of the solar simulator for three light treatments: no extra light screening (i.e., full spectrum, FS), screened by the Mylar-D filter (UVB excluded), and screened by the UF-5 Plexiglas filter (both UVA and UVB excluded). Also shown is the monthly-averaged clear-sky noontime solar irradiance spectrum in January 2016 at 22.5°N derived from the SMARTS2 model.[1,2]

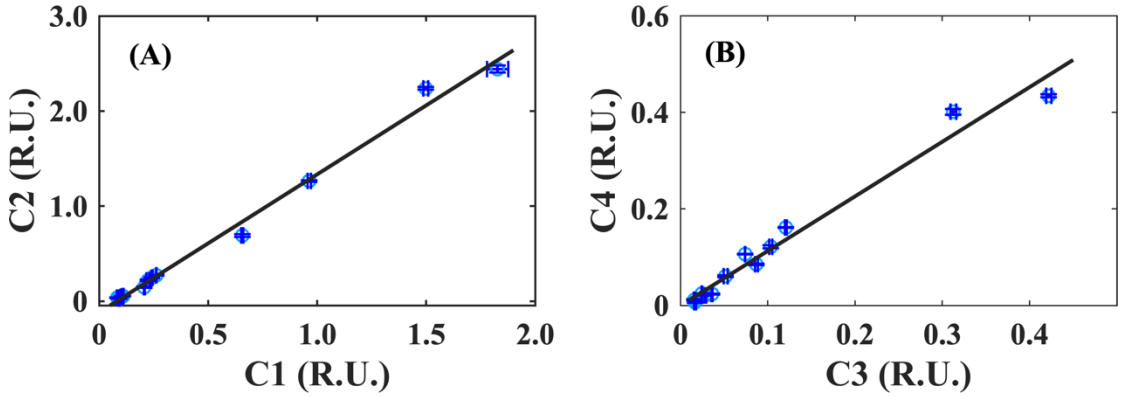

Figure S2. Plots of C2 versus C1 (A) and C4 versus C3 (B). The straight lines are the linear-regression lines, with the mathematical forms of C2 = 1.451C1- 0.117, R^2 = 0.992, $p < 0.01$; C4= 1.132C3 - 0.00004, R^2 = 0.973, $p < 0.05$.

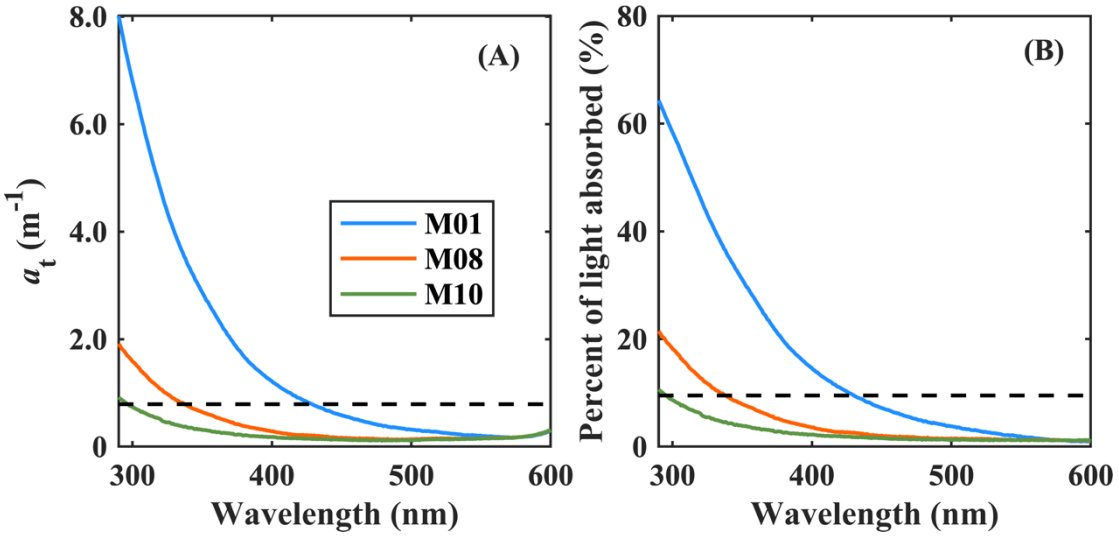

Figure S3. a_t (A) and percent of light absorbed by a sample (B) in the irradiation vessel as a function of wavelength for the original water samples. In panel A, a_t is the sum of the absorption coefficient of CDOM and pure water.[4,5] Based on Hu et al. (2002)[13], we define the system as being optically thin when $a_t \times L < 0.1$ (L is the light pathlength) and not optically thin when at $\times L > 0.1$. As the height of the quartz vessels (i.e., L) was 0.13 m, significant self-shading existed when at and the light absorption exceeded 0.77 m^{-1} and 9.5% (black dashed lines in panels A and B), respectively. Self-shading was significant at wavelengths < 428 nm for the M01 sample, < 336 nm for the M08 sample and < 296 nm for the M10 sample. Self-shading should have decreased during irradiation due to CDOM photobleaching.

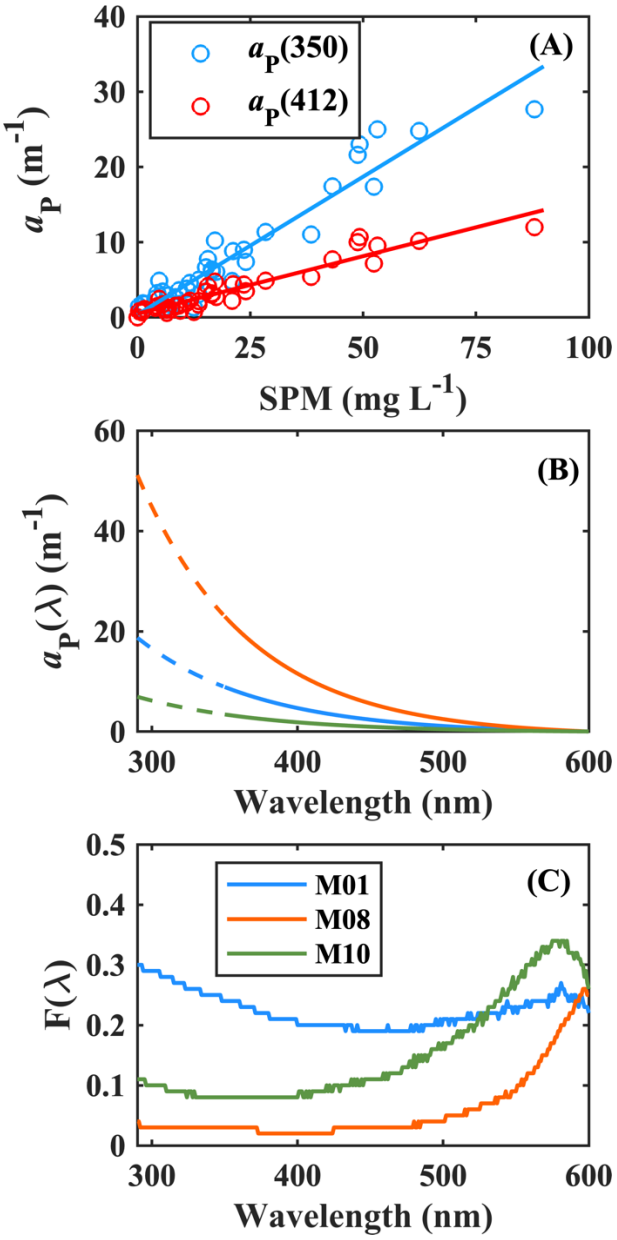

Figure S4. Typical absorption coefficients of particles versus SPM concentration based on samples collected in July 2013[7] (A); the retrieved absorption spectra of particles (B); and the calculated fraction of photons absorbed by CDOM (C) at Sta. M01, M08 and M10 in January 2016. In panel B: the dashed lines are the extrapolated values based on the regressed equations of $a_p(\lambda)$ versus wavelength: $a_p(\lambda) = 619.1 \times e^{(-0.01199\lambda)} - 0.416$ (M01); $a_p(\lambda) = 2250 \times e^{(-0.01299\lambda)} - 0.895$ (M08); $a_p(\lambda) = 1927 \times e^{(-0.01137\lambda)} - 0.175$ (M10). In panel C: F(λ) denotes the fraction of photons absorbed by CDOM within the wavelength range of 290–600 nm.

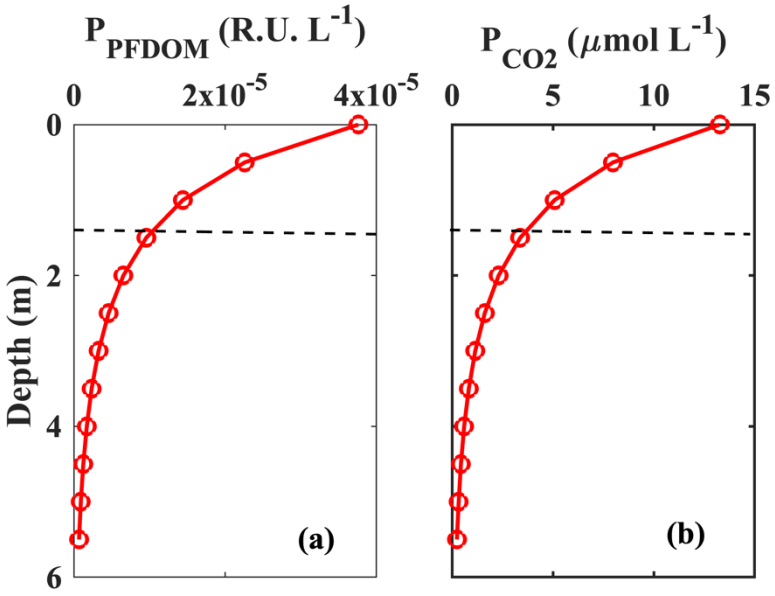

Figure S5. Modelled VIS-induced monthly photoproduction of protein-like FDOM (A) and CO_2 (B) in the water column in January 2016. The dashed horizontal line indicates the 1% UVA penetration depth (1.4 m).

Table S1. The input conditions for modelling the surface solar irradiance at 22.5°N in January 2016 over the PRE.

Card ID	Input	Remark
Card 1	PRE201601	Title for current modelling
Card 2	1	Pressure of the site
Card 2a	1013.25, 0, 0	Pressure, altitude, height
Card 3	1	Proper default atmosphere
Card 3a	STW	Sub-tropical winter
Card 4	1	Default value for water vapor
Card 5	1	Default value for zone abundance
Card 6	1	Default values for all other gas abundances
Card 7	408	CO_2 concentration
Card 7a	0	Synthetic spectrum recently proposed[14]
Card 8	S&F_MARIT	Aerosol model
Card 9	0	Turbidity selection
Card 9a	0.084	Turbidity coefficient
Card 10	2	Zonal albedo, 2 denotes water or calm ocean
Card 10b	0	No correction for titled surface calculations
Card 11	280, 700, 1.034, 1367.0	280 and 700 are the minimum, maximum of the spectral range in nm, 1.034 is the correction factor of true sun-earth distance in January, 1367.0 is the selected solar constant (W/m^2)
Card 12	2	Spectral results are printed to file 17
Card 12a	280, 700, 1.0	280, 700 and 1.0 are the minimum, maximum and interval of the output solar spectrum in nm
Card 12b	5	Number of variables to print
Card 12c	2, 8, 9, 12, 38	Selected output variables
Card 13	0	No calculation of circumsolar radiation
Card 13a	0, 0, 0	They are the slope angle, half aperture angle and limit angle and limit angle of the simulated radiometer (we chose default values here)
Card 14	0	No scanning/smoothing virtual filter of the postprocessor
Card 15	0	No illuminance, luminous efficacy and PAR calculations
Card 16	0	No special UV calculation
Card 17	3	Inputs are year, month, day, hour, latitude, longitude and zone
Card 17a	2016, 1, 15, 5, 22.5, 113.5, 8	One example of above parameters (Card 17)

Table S2. *p* values of one-tailed t-tests for comparing the irradiated sample and the parallel dark control under FS, UVA+VIS and VIS.

	M01	M08	M10
	DOC		
FS	< 0.01	< 0.01	< 0.01
UVA+VIS	< 0.01	< 0.01	< 0.05
VIS	< 0.01	< 0.01	< 0.05
	$a_{CDOM}(330)$		
FS	< 0.01	< 0.01	< 0.01
UVA+VIS	< 0.01	< 0.05	< 0.05
VIS	< 0.05	> 0.05	> 0.05
	C_P		
FS	< 0.01	< 0.01	< 0.05
UVA+VIS	< 0.01	< 0.01	< 0.05
VIS	< 0.01	< 0.01	< 0.05
	C_H		
FS	< 0.01	< 0.01	< 0.01
UVA+VIS	< 0.01	< 0.01	< 0.05
VIS	< 0.05	> 0.05	> 0.05
	$a^*_{CDOM}(254)$		
FS	< 0.01	< 0.01	< 0.01
UVA+VIS	< 0.01	< 0.05	> 0.05
VIS	< 0.01	< 0.05	> 0.05
	$S_{275\text{-}295}$		
FS	< 0.01	< 0.01	< 0.01
UVA+VIS	< 0.05	< 0.01	< 0.05
VIS	> 0.05	> 0.05	< 0.05
	$S_{300\text{-}600}$		
FS	< 0.01	< 0.01	< 0.01
UVA+VIS	< 0.01	< 0.01	< 0.05
VIS	< 0.01	< 0.05	< 0.05

Table S3. *p* values of two-tailed t-tests for comparing samples irradiated under FS, UVA+VIS and VIS.

	M01 vs M08	M08 vs M10	M01 vs M10
		DOC	
FS	< 0.01	> 0.05	< 0.01
UVA+VIS	< 0.01	> 0.05	< 0.01
VIS	> 0.05	> 0.05	> 0.05
		$a_{CDOM}(330)$	
FS	< 0.01	< 0.05	< 0.01
UVA+VIS	< 0.01	< 0.05	< 0.01
VIS	> 0.05	> 0.05	> 0.05
		C_P	
FS	< 0.01	< 0.01	< 0.01
UVA+VIS	< 0.01	> 0.05	< 0.01
VIS	< 0.01	< 0.01	< 0.01
		C_H	
FS	< 0.01	< 0.01	< 0.01
UVA+VIS	< 0.01	< 0.05	< 0.01
VIS	> 0.05	> 0.05	> 0.05
		$a^*_{CDOM}(254)$	
FS	< 0.01	> 0.05	< 0.01
UVA+VIS	< 0.05	> 0.05	< 0.01
VIS	> 0.05	> 0.05	< 0.05
		$S_{275-295}$	
FS	< 0.01	> 0.05	< 0.05
UVA+VIS	< 0.05	> 0.05	> 0.05
VIS	< 0.05	< 0.05	< 0.05
		$S_{300-600}$	
FS	< 0.01	< 0.01	< 0.01
UVA+VIS	> 0.05	< 0.05	< 0.05
VIS	> 0.05	> 0.05	> 0.05

Table S4. *p* values of two-tailed t-tests for comparing samples irradiated under FS, UVA and VIS.

Light treatment	M01 vs M08	M08 vs M10	M01 vs M10
		AQY_{DOC}	
FS	> 0.05	> 0.05	> 0.05
UVA	< 0.05	> 0.05	> 0.05
VIS	> 0.05	> 0.05	> 0.05
		AQY_{CDOM}	
FS	> 0.05	> 0.05	> 0.05
UVA	> 0.05	> 0.05	> 0.05
VIS	> 0.05	> 0.05	> 0.05
		AQY_{PFDOM}	
FS	< 0.05	< 0.01	< 0.01
UVA	< 0.01	> 0.05	< 0.01
VIS	< 0.01	< 0.05	< 0.01
		AQY_{HFDOM}	
FS	> 0.05	< 0.05	< 0.01
UVA	> 0.05	> 0.05	< 0.01
VIS	> 0.05	> 0.05	> 0.05

References:

1 C. Gueymard, SMARTS (version 2.9.5), SMARTS, A Simple Model of the Atmospheric Radiative Transfer of Sunshine: Algorithms and Performance Assessment. *Professional Paper FSEC-PF-270-95,* Florida Solar Energy Center, FL, 1995.

2 C. Gueymard, Parameterized Transmittance Model for Direct Beam and Circumsolar Spectral Irradiance, *Solar Energy*, 2001, **71**(5), 325–346.

3 A. Stubbins, G. Uher, C. S. Law, K. Mopper, C. Robinson, and R. C. Upstill-Goddard, Open-ocean carbon monoxide photoproduction, *Deep-Sea Res. PT II*, 2006, **53**, 1695–1705.

4 H. Buiteveld, J. M. H. Hakvoort, and M. Donze, The optical properties of pure water, *Proc. SPIE*, 1994, **2258**, Ocean Opt. XII., 174–183.

5 R. M. Pope, and E. S. Fry, Absorption spectrum (380–700 nm) of pure water. II. Integrating cavity measurements, *Appl. Opt.*, 1997, **36**(33), 8710–8723.

6 R. Li, J. Xu, X. Li, Z. Shi, and P. J. Harrison, Spatiotemporal variability in phosphorus species in the Pearl River estuary: Influence of the river discharge, *Sci. Rep.*, 2017, **7**, 13649, doi:10.1038/s41598-017-13924-w

7 S. Wang, Y. Wang, Q. Fu, B. Yin, and Y. Li, Spectral absorption properties of the water constituents in the estuary of Zhujiang River, *Environ.Sci.* 2014, **35**(12), 4511–4521. (in Chinese)

11 C. Hu, F. E. Muller-Karger, and R. G. Zepp, Absorbance, absorption coefficient, and apparent quantum yield: A comment on common ambiguity in the use of these optical concepts, *Limnol. Oceanogr.*, 2002, **47**(4), 1261–1267.

8 W. L. Miller, and M. A. Moran, Interaction of photochemical and microbial processes in the degradation of refractory dissolved organic matter from a coastal marine environment, *Limnol. Oceanogr.*, 1997, **42**(6), 1317–1324.

9 E. M. White, D. J. Kieber, J. Sherrard, W. L. Miller, and K. Mopper, Carbon dioxide and carbon monoxide photoproduction quantum yields in the Delaware estuary, *Mar. Chem.*, 2010, **118**, 11–21.

10 A. Morel, Optical properties of pure water and pure seawater, in *Optical Aspects of Oceanography*, ed. N. G. Jerlov, and E. S. Nielsen, Academic Press, New York, 1974, chapter 1, pp. 1–24.

12 A. Vodacek, S. A. Green, and N. V. Blough, An experimental model of the solar-stimulated fluorescence of chromophoric dissolved organic matter, *Limnol. Oceanogr.*,1994, **39**(1), 1–11.

13 S. Buckley, F. Leresche, K. Norris, and F. L. Rosario-Ortiz, Role of direct and sensitized photolysis in the photomineralization of dissolved organic matter and model chromophores to carbon dioxide, *Environ. Sci. Technol.*, 2024, **58**(31), 13808–13819.

14 C. Gueymard, The sun's total and spectral irradiance for solar energy applications and solar radiation models, *Sol. Energy*, 2004, **76**, 423–453.